

# Detection of H I in distant galaxies using spectral stacking

J. Delhaize<sup>1\*</sup>, M. J. Meyer<sup>1,2</sup>, L. Staveley-Smith<sup>1,2</sup>, B. J. Boyle<sup>2,3</sup>

<sup>1</sup>*International Centre for Radio Astronomy Research (ICRAR), M468, University of Western Australia, 35 Stirling Hwy, Crawley, WA, 6009, Australia*

<sup>2</sup>*ARC Centre of Excellence for All-sky Astrophysics (CAASTRO)*

<sup>3</sup>*CSIRO Astronomy and Space Science, PO Box 76, Epping, NSW 1710, Australia*

Accepted 2013 May 8. Received 2013 May 6; in original form 2013 February 23

## ABSTRACT

Using the Parkes radio telescope, we study the 21 cm neutral hydrogen (H I) properties of a sample of galaxies with redshifts  $z < 0.13$  extracted from the optical Two-Degree-Field Galaxy Redshift Survey (2dFGRS). Galaxies at  $0.04 < z < 0.13$  are studied using new Parkes observations of a  $42 \text{ deg}^2$  field near the South Galactic Pole (SGP). A spectral stacking analysis of the 3,277 2dFGRS objects within this field results in a convincing  $12 \sigma$  detection. For the low-redshift sample at  $0 < z < 0.04$ , we use the 15,093 2dFGRS galaxies observed by the H I Parkes All-Sky Survey (HIPASS) and find a  $31 \sigma$  stacked detection. We measure average H I masses of  $(6.93 \pm 0.17) \times 10^9$  and  $(1.48 \pm 0.03) \times 10^9 h^{-2} M_{\odot}$  for the SGP and HIPASS samples, respectively. Accounting for source confusion and sample bias, we find a cosmic H I mass density of  $\Omega_{\text{H I}} = (3.19^{+0.43}_{-0.59}) \times 10^{-4} h^{-1}$  for the SGP sample and  $(2.82^{+0.30}_{-0.59}) \times 10^{-4} h^{-1}$  for the HIPASS sample. This suggests no ( $12 \pm 23$  per cent) evolution in the cosmic H I density over the last  $\sim 1 h^{-1}$  Gyr. Due to the very large effective volumes, cosmic variance in our determination of  $\Omega_{\text{H I}}$  is considerably lower than previous estimates. Our stacking analysis reproduces and quantifies the expected trends in the H I mass and mass-to-light ratio of galaxies with redshift, luminosity and colour.

**Key words:** galaxies: evolution – galaxies: ISM – radio lines: galaxies

## 1 INTRODUCTION

To obtain a complete picture of galaxy evolution, it is crucial to understand how the cold gas content of galaxies varies with cosmic time. Cold gas ( $< 10^4$  K), largely in the form of neutral hydrogen (H I), is supplied through various accretion, merger and feedback processes (eg. Kereš et al. 2005) and is later available to condense into massive molecular clouds and stars. Without this gas, star formation is quenched and evolution continues only passively. To improve our understanding of the evolution in quantities such as star formation rate density (Madau et al. 1996, Hopkins & Beacom 2006), it is therefore fundamental to also improve our understanding of changes in the cosmic gas density.

Models that attempt to predict the variation of cosmic gas density with redshift diverge in their predictions. This is partly due to the wide spatial range required to track the requisite gas physics and partly because of uncertainty in the physics of galaxy formation, in particular the action of feedback from stars and AGN (eg. Somerville et al. 2001; Cen et al. 2003; Nagamine et al. 2005; Power et al. 2010;

Lagos et al. 2011). Thus, observational constraints are vital.

A number of observational techniques exist for tracing H I gas within galaxies. At high redshifts, the Gunn-Peterson effect applied to damped Lyman  $\alpha$  (DLA) systems can be exploited. Prochaska et al. (2005) and Prochaska & Wolfe (2009) used Sloan Digital Sky Survey (SDSS) spectra to trace systems with H I column densities above  $2 \times 10^{20} \text{ cm}^{-2}$  at  $z > 1.7$ . Though they find a statistically significant detection of evolution in the cosmic H I density within  $2.2 < z < 3.5$ , interpretation of their results is problematic due to systematic effects such as dust obscuration and gravitational lensing. At  $z < 1.65$  the Lyman  $\alpha$  transition is observed at ultraviolet wavelengths, making it difficult to trace with the limited time available on space-based observatories. Rao et al. (2006) were able to contribute in this regime by optically identifying DLA systems through metal absorption lines in SDSS data. They found no evidence of evolution in the cosmic H I density of DLAs within  $0.5 < z < 5$ , although their results are limited by statistical uncertainty.

The preferred method for tracing H I in the local Universe ( $z \approx 0$ ) is via the direct detection of the neutral hydrogen 21 cm hyperfine emission line. With the wide instantaneous field of view provided by multibeam receivers on large radio telescopes, it is feasible to conduct blind,

\* E-mail: jacinta.delhaize@icrar.org

all-sky surveys at 21 cm. This has facilitated the detection of H I in large numbers of galaxies. A prime example of this is the H I Parkes All-Sky Survey (HIPASS), conducted with the 64 m Parkes radio telescope in New South Wales, Australia (Barnes et al. 2001; Staveley-Smith et al. 1996). HIPASS detected H I within 5,317 galaxies at  $0 < z < 0.04$  (Meyer et al. 2004; Wong et al. 2006), allowing the construction of the most reliable and complete H I mass function then available, and an estimate of the H I mass density for the local Universe (Zwaan et al. 2005). Similarly, the Arecibo Legacy Fast ALFA (ALFALFA) survey aims to detect >30,000 galaxies at 21 cm out to  $z = 0.06$  over a sky area of  $\sim 7,000 \text{ deg}^2$  (Giovanelli et al. 2005). Using the 40 per cent ALFALFA catalogue, Martin et al. (2010) find a cosmic H I mass density 16 per cent higher than that derived by Zwaan et al. (2005). They conclude that this discrepancy is caused by an under-representation in the HIPASS catalogue of the rare, high-mass [ $9.0 < \log(M_{\text{HI}}/M_{\odot}) < 10.0$ ] galaxies due to sensitivity limits.

Deeper, blind H I surveys are underway, such as the Arecibo Ultra Deep Survey (AUDS). This survey aims to directly detect significant numbers of field galaxies out to  $z = 0.16$  to probe the evolution of cosmic H I properties (Freudling et al. 2011). However, the survey time required to achieve sufficient sensitivity at these higher redshifts restricts the observations to a narrow field ( $1/3 \text{ deg}^2$  for AUDS), thus potentially introducing a strong cosmic variance bias.

To date, the deepest detections of 21 cm emission in individual galaxies have been made at  $z \approx 0.2$  by Catinella et al. (2008) using pointed observations with the sensitive 305 m Arecibo telescope, and by Zwaan et al. (2001) and Verheijen et al. (2007) using long integrations of cluster galaxies with the Westerbork Synthesis Radio Telescope (WSRT). While future instruments such as the Square Kilometre Array (SKA) and its pathfinders should have the ability to detect 21 cm emission to much higher redshifts over large sky areas, these will not be available for a number of years.

However, methods other than direct, individual detections are available to push the current redshift limit of H I observations. In particular, stacking is a useful method for probing H I within large samples of distant galaxies. Stacking is the process of co-adding individual non-detections in an attempt to boost the signal-to-noise ratio (S/N) of the data and thereby recover a more significant statistical detection.

Zwaan (2000), Chengalur et al. (2001) and Lah et al. (2009) demonstrated that stacking can be successfully used to examine the environmental influence on the H I properties of cluster galaxies out to  $z = 0.37$ . Lah et al. (2007) were the first to apply this co-adding method to field galaxies to study the evolution of the cosmic H I density. They examined 154 star-forming galaxies selected in H $\alpha$  at  $z = 0.24$  using 21 cm data from the Giant Metrewave Radio Telescope (GMRT); however, averaged detections were  $3\sigma$  at best.

Fabello et al. (2011a) and Fabello et al. (2011b) used similar stacking methods to examine the impact of bulge presence and AGN activity on the H I content of galaxies with stellar masses greater than  $10^{10} M_{\odot}$ . They demonstrated that when using relatively low redshift ( $0.025 < z < 0.05$ ) H I data and a large sample of galaxies, strong stacked

detections were possible, even for the subsample of galaxies individually undetected at 21 cm.

The related technique of ‘intensity mapping’, which uses cross-correlation of radio and optical redshift data, has been used by Pen et al. (2009), Chang et al. (2010) and Masui et al. (2013) to detect H I in samples at even higher redshift.

The work presented here aims to constrain the cosmic density of H I out to  $z = 0.13$  and demonstrate the accuracy of the stacking method over this redshift range. We have employed the fast survey speed of the Parkes telescope to collect 21 cm observations of a very large sample of field galaxies from the Two-Degree-Field Galaxy Redshift Survey (2dFGRS). The sample selection is not biased by environment, star formation signatures, or any particular physical characteristic other than the optical magnitude limits of the 2dFGRS. By using the wide but low-redshift HIPASS data, in combination with new, spectrally deep Parkes observations of a smaller subsection of the 2dFGRS footprint, we can examine the H I content of galaxies over the full range  $0 < z < 0.13$ .

Section 2 of this paper presents the optical redshift survey and the radio observations used in the analysis. The source selection and stacking procedures are described in Section 3. In Section 4.1 we present an analysis of noise behaviour in the H I data. Section 4.2 discusses the influence of source confusion on our results and illustrates how we correct for this. Section 4.3 describes the H I mass density calculation and Section 4.4 considers the impact of cosmic variance. Trends in H I properties with redshift, luminosity and colour are measured in Section 4.5. Finally, we present our conclusions in Section 5. We have assumed a  $\Lambda$  cold dark matter cosmology with a reduced Hubble constant  $h = H_0/(100 \text{ km s}^{-1} \text{ Mpc}^{-1}) = 1.0$ ,  $\Omega_{\Lambda} = 0.7$  and  $\Omega_{\text{M}} = 0.3$ .

## 2 THE DATA

### 2.1 The 2dFGRS optical catalogue

The basic principle of the H I stacking analysis employed here is to identify the positions and redshifts of galaxies using an external source catalogue containing optical redshifts, extract the H I information at these coordinates and then co-add the data. For the present analysis, the positions and redshifts are provided by the 2dFGRS. The 2dFGRS is a spectroscopic survey of over 250,000 galaxies conducted with the 2dF multifibre spectrograph on the Anglo-Australian Telescope. This survey covers two large strips, one in the Northern Galactic hemisphere and one in the south, as well as a number of small, random fields. The total sky coverage is  $\sim 2,000 \text{ deg}^2$ . See Colless et al. (2001) for further details of the surveyed regions.

The input photometric source catalogue for this survey comes from an adapted catalogue of Automated Plate Measuring (APM) machine scans of the Southern Sky Survey taken with the UK Schmidt Telescope. These target sources have extinction-corrected magnitudes brighter than  $b_J = 19.45$ . All APM  $b_J$  magnitudes used in this paper are extinction-corrected, but not ( $k + e$ )-corrected for bandpass and evolution. These corrections will be incorporated into the corresponding redshifted luminosity density.

As described in Colless et al. (2001), the redshifts were estimated using a combination of automated absorption spectral shape fitting, emission line identification and manual input. Each redshift was assigned a quality factor  $Q$  between 1 (no reliable redshift available) and 5 (very reliable redshift). We find that sources with  $Q \geq 3$  are sufficient for our stacking analysis. Colless et al. (2001) state that  $Q \geq 3$  redshifts have a root-mean-square (rms) uncertainty of  $85 \text{ km s}^{-1}$  and can be used with 98.4 per cent reliability.

## 2.2 H I observations and data

### 2.2.1 South Galactic Pole observations

We conducted a 21 cm survey with the 64 m Parkes radio telescope over a  $42 \text{ deg}^2$  ( $7^\circ \times 8^\circ$ ) sky field centred on right ascension (RA)  $00^{\text{h}}42^{\text{m}}00^{\text{s}}$  and declination (Dec.)  $-29^\circ00'00''$  (J2000), close to the South Galactic Pole (SGP). The region was chosen as it contains an overdensity of available 2dFGRS spectra (described further in Section 3.1). This provides a high number of spectra per square degree available for a stacking analysis. 87 h of telescope time was used for observations of this field. These were conducted on 2008 November 20-25, 2009 August 17-20 and 2009 September 25-29 with an estimated 52 h of on-source integration.

The observations used the multibeam correlator with two adjacent frequency bands, each with 1024 spectral channels over a bandwidth of 64 MHz. The bands were centred on 1285 and 1335 MHz with a 14 MHz overlap to reduce the impact of the bandpass shape. Observations in the two frequency bands were taken independently. The full frequency coverage of the Parkes data is thus 1253-1367 MHz over two polarizations. We therefore have the potential to detect galaxies with 21 cm redshifts in the range  $0.0391 < z < 0.1336$ . The resulting channel spacing is 62.5 kHz.

### 2.2.2 HIPASS observations

We also present a study using all overlapping data from the 2dFGRS catalogue and HIPASS. HIPASS was also conducted with the Parkes 64 m dish using the 21 cm multibeam receiver (Staveley-Smith et al. 1996) and covers the entire sky south of Dec.  $+25^\circ$ . The HIPASS velocity range is  $-1280 < cz < 12700 \text{ km s}^{-1}$ , corresponding to a frequency coverage of 1362.5–1426.5 MHz and redshifts below  $z = 0.0423$ . Observations of the southern field (below Dec.  $+2^\circ$ ) were completed over the period from 1997 February to 2000 March (Barnes et al. 2001). The northern field (Dec.  $+2^\circ$  to  $+25^\circ$ ) was observed from 2000 to 2002 (Wong et al. 2006). The HIPASS and SGP data sets overlap by only 4.5 MHz ( $\Delta z = 0.003$ ) in spectral range, making the two data sets highly complementary.

### 2.2.3 Telescope scanning mode

Both data sets were collected using a similar Parkes scanning mode, where the telescope is actively scanned across the required sky area at a rate of  $1^\circ \text{ min}^{-1}$ . While HIPASS only used scans in declination, the SGP observations used a ‘basket-weave’ pattern, with the entire field also covered

by right ascension scans. This reduces the effect of negative sidelobes around bright continuum sources created by the bandpass correction. Using this technique, the SGP field was completely surveyed 15 times in each spectral band within the available time frame.

### 2.2.4 Data reduction and interference mitigation

Bandpass removal and calibration were conducted identically for both data sets using the LIVEDATA<sup>1</sup> reduction package. See Barnes et al. (2001) for a detailed explanation of these processes. The data were smoothed to reduce the effects of ringing created by strong Galactic emission and/or strong radio frequency interference (RFI), such as from satellites. Hanning smoothing was applied to the SGP data. HIPASS utilized Tukey 25 per cent smoothing. However, we have also applied Hanning smoothing to the data for consistency. The spectral resolution after smoothing is 125 kHz ( $26.4 \text{ km s}^{-1}$  at  $z = 0$ ).

The use of robust statistics in HIPASS data processing (see Section 2.2.5 below) was sufficient to mitigate against the majority of RFI. However, the lower frequencies probed during SGP observations suffer from greater RFI. To improve the quality of the SGP data, we applied an automated RFI masking routine to the reduced, smoothed data. The mean and rms noise levels were calculated in an RFI-free region and the resultant  $3\sigma$  clipping threshold was set at 250.5 mJy. All pixels with absolute deviations above this threshold were masked. This was not sufficient to completely mitigate against the presence of strong satellite RFI in the frequency range 1262.4–1276.8 MHz. It was not consistently present and appears in 24 per cent of the observations in the 1285 MHz band. Therefore, the full range of affected channels was completely masked in all data files containing this RFI. This method was successful in recovering only the good quality data in the broad-band RFI zone. In addition, all data in channels around 1280, 1300, 1312, 1316, and 1350 MHz were masked as they were also completely contaminated by satellite RFI. The resulting fraction of flagged data per channel is shown in Fig. 1.

### 2.2.5 Gridding

The reduced Parkes data were gridded using GRIDZILLA<sup>2</sup>. Robust median averaging was used to minimize the impact of RFI on the final cubes and the two polarizations were added. Pixel sizes in the gridded data are each  $4 \times 4 \text{ arcmin}^2$ . For more details, see Barnes et al. (2001).

The SGP field is sufficiently small that it is reasonable to produce a single cube in each frequency band. To account for the band overlap, each cube was cut at 1310 MHz and the two were then concatenated together such that the frequency coverage was continuous. The rms noise per channel in the RFI-free part of the final data cube is  $8.5 \text{ mJy beam}^{-1}$ . The

<sup>1</sup> LIVEDATA is supported by the Australia Telescope National Facility and is available at <http://www.atnf.csiro.au/computing/software/livedata/>

<sup>2</sup> GRIDZILLA is supported by the Australia Telescope National Facility and is available at <http://www.atnf.csiro.au/computing/software/livedata/>

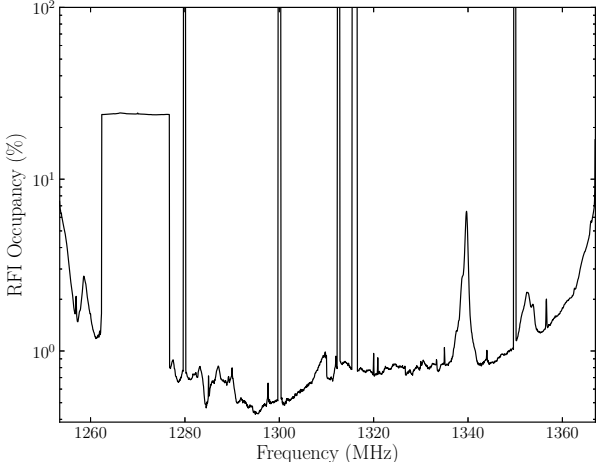


**Figure 1.** The percentage of low-quality SGP data excluded in each frequency channel, largely due to the presence of satellite RFI.

flux density scale is calibrated against 1934-638 and Hydra A. Calibrations are consistent to within  $\sim 2$  per cent.

Since the sky coverage of the HIPASS data is so large, the southern region is split into 388 separate sky fields, each measuring  $8 \times 8 \text{ deg}^2$  (Barnes et al. 2001). The northern HIPASS field consists of 102  $8 \times 8 \text{ deg}^2$  cubes and 48  $8 \times 7 \text{ deg}^2$  cubes (Wong et al. 2006). The rms noise level of the HIPASS data is 13.3 mJy (Barnes et al. 2001), which is 56 per cent higher than the SGP data. The effective spatial resolution of both the gridded SGP and HIPASS data sets is 15.5 arcmin.

### 3 ANALYSIS

#### 3.1 SGP source selection

There are 4,240 2dFGRS sources in the SGP field with high-quality redshifts ( $Q \geq 3$ ) covered by the 21 cm observations. However, not all of these are suitable for use in this stacking analysis. All channels within 2 MHz of the extremes of the spectral range were discarded due to the bandpass shape, and the corresponding sources rejected. Therefore, we have a final redshift coverage of  $0.0405 < z < 0.1319$  for this SGP sample. Additionally, sources were rejected from the sample if their redshifted H I signatures fell at frequencies with 100 per cent RFI occupancy in the data (see Fig. 1).

Continuum sources must be avoided as they can induce standing waves in the data (Barnes et al. 2001) and create a discontinuity between the two spectral bands. Using the NRAO VLA Sky Survey (NVSS) source catalogue by Condon et al. (1998), the 17 continuum sources in the SGP field with 1.4 GHz flux densities greater than 200 mJy were identified. The 840 2dFGRS galaxies with angular separations from these continuum sources of less than the spatial resolution of the data were discarded from the sample.

Our final 2dFGRS sample therefore contains 3,277 sources suitable for stacking within the SGP field. The heliocentric redshift distribution of these sources is shown in Fig. 2. Many galaxies are distributed around  $z = 0.11$  and the average redshift of the sample is 0.096. This ‘clumpiness’

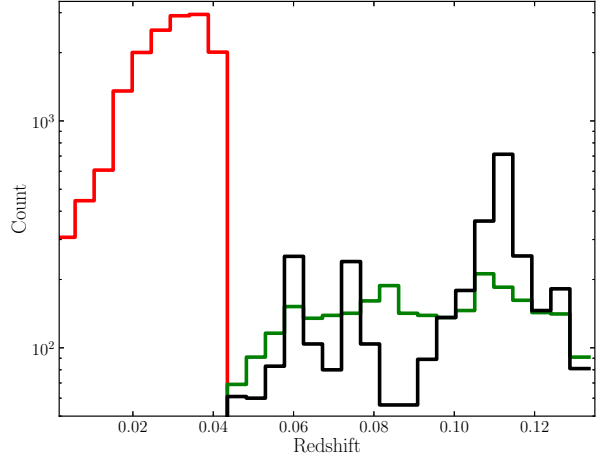


**Figure 2.** The heliocentric redshift distributions of the optical samples considered here. The black line shows the 3,277 2dFGRS sources within the observed SGP region and spectral range suitable for stacking. Overlaid in green is the redshift distribution of the full 2dFGRS catalogue across this redshift range, scaled by the ratio of the SGP to total 2dFGRS field areas. The red line shows the distribution of the 15,093 2dFGRS sources with available HIPASS spectra. The average redshift of this sample is 0.029.

in redshift space is not attributable to a single galaxy cluster, but seems to be probing genuine cosmic structure. For example, the 2dFGRS Percolation-Inferred Galaxy Group (2PIGG) catalogue by Eke et al. (2004) identifies 17 galaxy groups with 10 or more members at  $z \approx 0.11$  within the SGP region.

For comparison, the redshift distribution of the full 2dFGRS catalogue (across the relevant  $z$  range) is also shown in Fig. 2. It has been scaled down by the ratio of the full 2dFGRS and SGP field areas so the shape of the two distributions can be compared. The full 2dFGRS distribution is far more uniform across redshift and the ratio of the total source counts reveals that the SGP field contains an  $\sim 30$  per cent overdensity at these redshifts. It is therefore evident that large-scale clustering is present in the chosen SGP field, highlighting the importance of cosmic variance considerations in such an analysis. This is discussed in detail in Section 4.4.

#### 3.2 HIPASS source selection

The full HIPASS completely covers the 2dFGRS footprint, but is limited in redshift coverage. There are 15,152 2dFGRS sources with reliable redshifts ( $Q \geq 3$ ) within the spectral range of the HIPASS data that are appropriate for stacking. This number excludes any sources with  $z < 0.0025$  ( $v < 750 \text{ km s}^{-1}$ ) to minimize contamination from the Galaxy and misclassified stars. We have removed the contribution of any Galactic emission from all spectra by masking frequency channels between 1418.4 and 1422.4 MHz. Our final HIPASS sample consists of 15,093 2dFGRS sources. The redshift distribution is shown in Fig. 2. According to Barnes et al. (2001), the contribution from continuum sources has already been suppressed in the HIPASS data by fitting a weighted

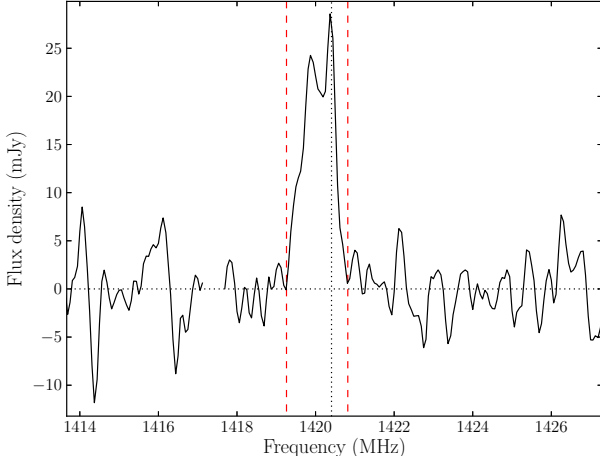


**Figure 3.** The 21 cm flux density spectrum of the only directly detected 2dFGRS source in the SGP field. The gap in the spectrum is due to RFI flagging. The dashed red lines show the nominal width of the profile and the vertical dotted line indicates the rest frequency.

Parameter	Value
RA (2dFGRS)	00:40:04.28
Dec. (2dFGRS)	-30:35:45.60
$z$ (2dFGRS)	0.0500
$\nu_{\text{centre}}$ (MHz)	1352.8
$\Delta v$ (km s $^{-1}$ )	329
S/N	7.2
$S_{\text{int}}$ (mJy MHz)	24
$M_{\text{HI}} (\times 10^9 h^{-2} M_{\odot})$	29

**Table 1.** Measured parameters of the SGP detection in Fig. 3.

average of the spectral shape near these sources and subtracting from all subsequent spectra.

### 3.3 Stacking process

#### 3.3.1 Extracting HI spectra

For each 2dFGRS source in our final sample, we extracted the full 21 cm spectrum from the data cube using an optimal weighting according to the beam shape, centred on the pixel corresponding to the RA and Dec. defined in the optical catalogue. This extraction strategy optimizes the S/N of the stacked spectrum but results in an expanded effective beam width of 21.2 arcmin ( $\sim 1.6 h^{-1}$  Mpc at  $z = 0.1$ ) for the SGP data and 21.9 arcmin ( $\sim 0.6 h^{-1}$  Mpc at  $z = 0.03$ ) for the HIPASS data.

We find one direct HI detection of a 2dFGRS source in the SGP sample with an S/N of 7.2. The HI spectrum of this source is shown in Fig. 3 and the measured parameters are reported in Table 1. There is no firm evidence of HI detection in the rest of the sample.

In contrast to this, there are numerous, significant individual detections in the HIPASS spectra owing to the fact that HIPASS surveys the more local Universe. The HIPASS source catalogue (HICAT) created by Meyer et al. (2004) (southern field) and Wong et al. (2006) (northern

field) identifies 5,317 HI sources in total. 226 of these coincide spatially and spectrally with 2dFGRS galaxies in our sample such that they will contribute to the extracted HI spectrum.

The HI mass per unit frequency in the observed frame (hereafter referred to as the mass spectrum  $M_{\text{HI},\nu_{\text{obs}}}$ ) can be calculated from:

$$\left( \frac{M_{\text{HI},\nu_{\text{obs}}}}{M_{\odot} \text{ MHz}^{-1}} \right) = 4.98 \times 10^7 \left( \frac{S_{\nu_{\text{obs}}}}{\text{Jy}} \right) \left( \frac{D_L}{\text{Mpc}} \right)^2, \quad (1)$$

where  $S_{\nu_{\text{obs}}}$  is the observed-frame HI flux density and  $D_L$  is the luminosity distance.

#### 3.3.2 Stacking spectra

The first step in the stacking process is to align all extracted spectra at rest frequency (1420.406 MHz). The spectral axis is converted from the observed to the emitted frame via  $\nu_{\text{em}} = \nu_{\text{obs}}(1+z)$ . To conserve the total mass (i.e.  $\int M_{\text{HI},\nu_{\text{em}}} d\nu_{\text{em}} = \int M_{\text{HI},\nu_{\text{obs}}} d\nu_{\text{obs}}$ ), the HI mass per unit frequency in the galaxy rest frame is given by

$$M_{\text{HI},\nu_{\text{em}}} = \frac{M_{\text{HI},\nu_{\text{obs}}(1+z)}}{(1+z)}. \quad (2)$$

The data around rest frequency now contain any HI emission associated with the galaxies. These  $n$  aligned spectra are then ‘stacked’ by finding the weighted mean in each channel:

$$\langle M_{\text{HI}} \rangle_{\nu_{\text{em}}} = \frac{\sum_{i=1}^n (w_i M_{\text{HI},\nu_{\text{em},i}})}{\sum_{i=1}^n w_i}, \quad (3)$$

where  $M_{\text{HI},\nu_{\text{em},i}}$  is the value of the  $i$ th mass spectrum at emitted frequency  $\nu_{\text{em}}$ . We choose the weighting factor  $w_i = \sigma_i^{-2}$  (where  $\sigma$  is the rms noise level of each observed-frame flux density spectrum), which improves the S/N of the final co-added spectrum. Using  $w_i = (\sigma_i D_i^2)^{-2}$  would further optimize the S/N but would reduce the effective volume and increase cosmic variance in our results.

The stacked spectra produced by co-adding all 3,277 SGP sources and 15,093 HIPASS sources are shown in Fig. 4. Although only one galaxy is individually detected in the SGP data, a strong  $12\sigma$  averaged detection is achieved through stacking. As expected, a more significant  $31\sigma$  stacked detection is achieved for the HIPASS sample due to the presence of many strong individual detections and a larger overall sample size.

The stacked SGP profile nominally spans the spectral range indicated by the dashed lines in Fig. 4 and is 1418.23 – 1421.97 MHz ( $\Delta v = 790 \text{ km s}^{-1}$ ). The stacked HIPASS profile spans 1418.83 – 1421.77 MHz ( $\Delta v = 621 \text{ km s}^{-1}$ ). These are significantly wider than the expected HI line widths of the individual galaxies contributing to the stack (see Section 4.2.1).

Possible explanations for the broadened stacked profiles include: (i) systematic differences between optical and radio redshifts, (ii) errors in the optical redshifts ( $85 \text{ km s}^{-1}$ ) and (iii) source confusion. The principle cause is likely confusion, particularly in the case of the higher redshift SGP data where a larger volume is probed per beam. This will be explored in detail in Section 4.2.

Note that the HIPASS spectrum is symmetric as expected, yet the SGP spectrum is  $\sim 0.62 \text{ MHz}$  ( $130 \text{ km s}^{-1}$ ) wider at frequencies below the rest frame. This does not appear to be related to optical redshift accuracy.

The green line in Fig. 4 indicates the noise level from averaged mock spectra created by stacking sources from a control catalogue. This catalogue was generated by randomly mismatching 2dFGRS redshifts and the source positions. By using the false redshifts in the extraction process, the channels shifted to  $1420.4 \text{ MHz}$  should not contain any H I emission. Thus, co-adding these mock spectra will not produce any stacked detection but will closely approximate the noise behaviour. A baseline was removed from all stacked spectra via fourth-order least-squares polynomial fitting over a  $14 \text{ MHz}$  spectral range, excluding the signal region.

### 3.3.3 Average H I mass

Integrating over the channels containing the stacked detection ( $\nu_{\text{em},1}$  to  $\nu_{\text{em},2}$ ) gives the average H I mass of the sample:

$$\langle M_{\text{H I}} \rangle = \int_{\nu_{\text{em},1}}^{\nu_{\text{em},2}} \langle M_{\text{H I}} \rangle_{\nu_{\text{em}}} d\nu_{\text{em}}. \quad (4)$$

We find average H I masses of  $\langle M_{\text{H I}} \rangle = (6.93 \pm 0.17) \times 10^9 h^{-2} M_{\odot}$  for the SGP sample and  $\langle M_{\text{H I}} \rangle = (1.48 \pm 0.03) \times 10^9 h^{-2} M_{\odot}$  for the HIPASS sample.

The error on the average mass is estimated by producing 10 control catalogues as in Section 3.3.2, repeating the stacking process for each, and then calculating the rms deviation in the integrated mass over the signal region.

In both cases, we appear to be sampling galaxies with average masses of less than  $M_{\text{H I}}^* = 8.4 \times 10^9 h^{-2} M_{\odot}$  (Zwaan et al. 2005). The  $5\sigma$  detection limit at the mean redshift of the SGP sample corresponds to an H I mass of  $\sim 1 \times 10^{11} h^{-2} M_{\odot}$ .

Note, however, that the average masses calculated here will be larger than the true value for each sample. This is due to significant source confusion in the data and will be discussed in Section 4.2. The significantly smaller mass obtained for the HIPASS sample is due to the 2dFGRS magnitude limit which allows more nearby, low-luminosity galaxies to appear, and due to less confusion with other galaxies in the telescope beam.

## 4 RESULTS

### 4.1 Noise behaviour

The best possible S/N achievable with a stacking analysis will be obtained if the noise behaves in a purely Gaussian manner and decreases with the square root of the number of co-added spectra. To demonstrate the noise behaviour

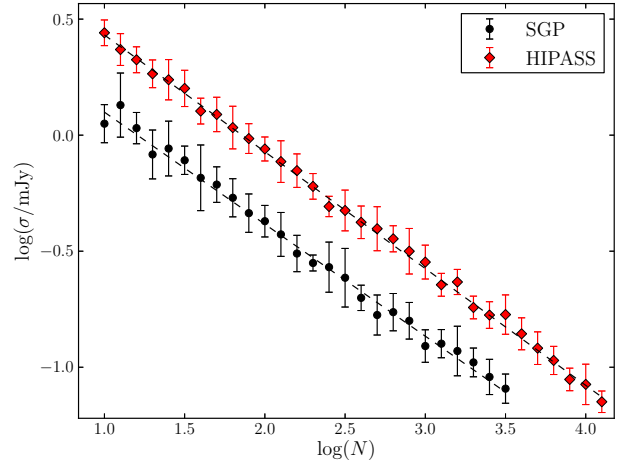


**Figure 5.** The rms noise level of the co-added spectrum versus the number of individual spectra contributing to the stack. The round black points are generated using SGP data and the red diamonds with HIPASS. The dashed lines show the best fit to the data. Both have gradients close to  $-0.5$ .

of the Parkes data, we stack  $N$  randomly selected spectra taken from the control catalogues described in Sections 3.3.2 and 3.3.3. Note that in this case we are stacking the flux density spectra, as opposed to the mass spectra. We then find the rms noise per channel calculated over the spectral range indicated by the dashed lines in Fig. 4.

Fig. 5 shows the noise level of the stacked spectrum as a function of the number of co-added spectra. It is evident that the noise within the signal region of the stacked 21 cm spectra in both data sets displays Gaussian behaviour, with gradients  $-0.48 \pm 0.05$  (SGP sample) and  $-0.50 \pm 0.03$  (HIPASS sample). This demonstrates that our data reduction has been successful in mitigating against non-Gaussian noise contributions from eg. RFI, residual continuum emission and insufficient bandpass calibration. If we do not apply these careful corrections to the data, we see evidence of a noise ‘floor,’ i.e. the sensitivity does not continue to decrease with the expected gradient, but flattens out once the non-Gaussian components begin to dominate.

We reach a final sensitivity of  $68 \mu\text{Jy}$  by stacking all 3,277 SGP spectra and  $68 \mu\text{Jy}$  by stacking all 15,093 HIPASS spectra. The integration time is  $975 \text{ s/pixel}$  in the SGP data and  $220 \text{ spixel}^{-1}$  in HIPASS (Barnes et al. 2001). This difference explains the vertical displacement of the SGP and HIPASS noise trends in Fig. 5. Despite the greater number of sources contributing to the final HIPASS stack, the longer integration time per pixel for the SGP data results in a similar final sensitivity. Observation of a single source for  $\sim 37 \text{ d}$  would be required to attain the same sensitivity as these final stacked spectra.

Note, however, that the mass spectra in Fig. 4 incorporate a  $D_L^2$  factor (see equation 1), which is larger for the higher redshift SGP sample. The rms noise level in the stacked SGP mass spectrum is therefore six times larger than for HIPASS.

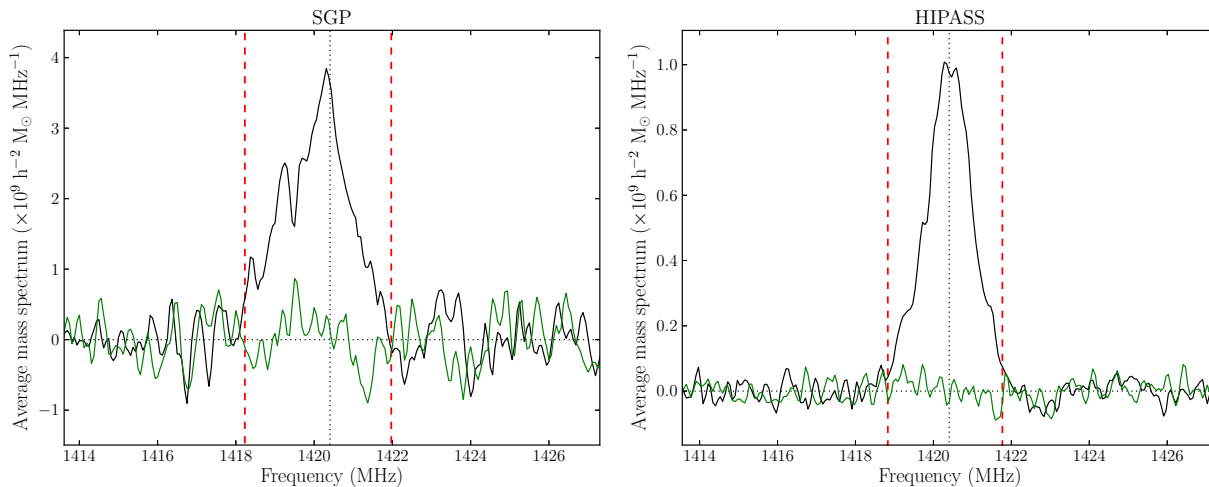


**Figure 4.** The co-added H I mass spectrum of all 3,277 SGP sources (left) and 15,093 2dFGRS sources covered by HIPASS (right). The vertical dotted line indicates the rest frequency of the H I line. The dashed red lines represent the nominal width of the stacked signal. The stacked spectrum generated using the control catalogue is shown in green to indicate the noise level in each case. A fourth-order polynomial baseline has been subtracted from all co-added spectra. Data between the dashed red lines were excluded when fitting baselines to the black spectra.

## 4.2 Confusion

The accuracy of the average quantities we measure via this stacking method will ultimately be limited by confusion in the Parkes data. We are unable to distinguish between multiple objects within the Parkes beam and therefore additional H I flux from neighbouring galaxies can contaminate our measurements.

Based on the simulated results of Obreschkow et al. (2013) and the observed H I line widths of HICAT galaxies, it is reasonable to assume a maximum line width of  $600 \text{ km s}^{-1}$  for any individual galaxy contributing to our analysis.

As discussed in Section 3.3.2 above, the stacked H I signals we achieve are broader than this, particularly for the SGP sample. Therefore, we consider all the flux in the wings of the stacked H I profile, beyond  $\pm 300 \text{ km s}^{-1}$  ( $\pm 1.42 \text{ MHz}$ ) from the rest frame, to exist solely due to confusion with other galaxies in the 2dFGRS catalogue, as well as fainter sources below its magnitude limit.

Restricting the integral in equation (4) to this spectral range would partially correct for confusion in the measured  $\langle M_{\text{H I}} \rangle$ . However, any flux within  $\pm 300 \text{ km s}^{-1}$  will still include contributions from confused sources, as well as from the target galaxies themselves. The challenge is therefore to identify which sources are confused over this spectral range, and then to correct for this.

### 4.2.1 Line width estimation with the Tully-Fisher relation

We do not directly detect the H I signature of many galaxies in our sample and so cannot determine their H I profile widths. Therefore, we cannot ascertain in advance whether we are integrating over single or multiple H I profiles and hence we cannot easily discern the extent of spectral confusion.

One way to overcome this is to estimate the H I line widths of each galaxy in our sample using the Tully-Fisher relation. We choose the  $B$ -band relation of Meyer et al.

(2008) which was derived using optical counterparts to HIPASS galaxies:

$$\log(v_{\text{rot}}) = -(M_B + 5 \log h + 1.4)/8.6, \quad (5)$$

where  $v_{\text{rot}}$  is the rotational velocity of the galaxy (in  $\text{km s}^{-1}$ ) and  $M_B$  is the  $B$ -band absolute magnitude.  $B$  apparent magnitudes are estimated from the SuperCOSMOS  $b_J$  and  $r_F$  apparent magnitudes available in the 2dFGRS catalogue as follows<sup>3</sup>:

$$B = b_J - 0.0047 + 0.236(b_J - r_F). \quad (6)$$

SuperCOSMOS magnitudes used in equation (6) have not been corrected for extinction by the Galaxy. However, we only require indicative values for  $B$  and  $v_{\text{rot}}$ . The H I line width  $W_{\text{H I}}$  (defined at 50 per cent peak flux) can then be estimated using:

$$W_{\text{H I}} = 2v_{\text{rot}} \sin(i), \quad (7)$$

where  $i$  is the inclination of the galaxy, calculated from the observed axial ratio as in equation (24) in Meyer et al. (2008). The distribution of the resulting line width estimates is shown in Fig. 6. The average width is  $150 \text{ km s}^{-1}$  for SGP and  $100 \text{ km s}^{-1}$  for HIPASS. This seems reasonable in comparison to the H I line widths of HICAT galaxies, which have an average of  $178 \text{ km s}^{-1}$ .

### 4.2.2 Identification of confused sources

Using the Tully-Fisher predicted line widths, we can now identify which 2dFGRS galaxies are likely to give rise to confusion over the spectral range of interest. We consider a

<sup>3</sup> Derived from magnitude conversions available at [www2.aao.gov.au/2dfgr/](http://www2.aao.gov.au/2dfgr/)

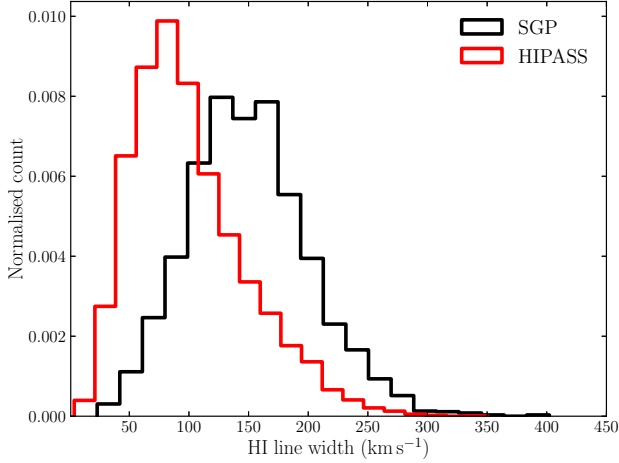


**Figure 6.** H I line widths estimated using the Tully-Fisher relation for the sample of SGP (black) and HIPASS (red) galaxies. Quantities have been normalized to show the relative spread in estimated line widths.

source confused with a particular target galaxy if: (i) it is within one beam width of the target galaxy ( $\pm 21.2$  arcmin for the SGP,  $\pm 21.9$  arcmin for HIPASS) and (ii) if any part of its predicted H I profile is within  $\pm 300 \text{ km s}^{-1}$  of the target galaxy’s recessional velocity.

As expected, we find significantly more confusion in the higher redshift SGP field. On average, any one SGP galaxy is confused with seven others. In the lower redshift HIPASS data, this decreases to three.

#### 4.2.3 Luminosity correction

The goal of this paper is to derive an estimate of H I density, based on the mass-to-light ratio of the galaxies. While we cannot fully correct  $\langle M_{\text{H I}} \rangle$  for confusion, we can account for this in the density estimate by artificially ‘confusing’ the optical luminosities. We do this by defining

$$L' = f \sum_{i=1}^n L_i b_i + L_0, \quad (8)$$

where  $L_0$  is the luminosity of the central galaxy,  $L_i$  are the luminosities of the  $n$  confused galaxies,  $b_i$  is the beam weighting factor defined using a Gaussian with full width at half maximum (FWHM)=21.2 arcmin (SGP) and FWHM=21.9 arcmin (HIPASS), and  $f$  is an extrapolation factor to account for luminosity from galaxies fainter than the 2dFGRS survey limit. The latter assumes the luminosity density function of Norberg et al. (2002), accounting for evolution and  $k$ -corrections.

Fig. 7 shows the original  $b_J$  luminosity distribution of each sample, compared to the confusion-adjusted luminosity distribution ( $L'$ ). The average (catalogued) luminosity for the SGP sample is  $6.62 \times 10^9 h^{-2} L_\odot$ . Once adjustment for confusion has been carried out, this average increases by a factor of 5 to  $3.36 \times 10^{10} h^{-2} L_\odot$ . The average original luminosity of the HIPASS sample is  $1.93 \times 10^9 h^{-2} L_\odot$ , which increases by a factor of 2.5 to  $4.87 \times 10^9 h^{-2} L_\odot$  when adjusted. As expected, the correction to the HIPASS lumi-

nosities is less significant to that of the SGP, due to less source confusion and a fainter absolute luminosity limit.

#### 4.3 H I mass density

The H I density,  $\rho_{\text{H I}}$ , can be calculated from the luminosity density and the mass-to-light ratio using

$$\rho_{\text{H I}} = \left\langle \frac{M_{\text{H I}}}{L} \right\rangle_{\rho_L} \times \rho_L, \quad (9)$$

as in eg. Fall & Pei (1993). We use the  $b_J$  luminosity density  $\rho_L = (1.82 \pm 0.17) \times 10^8 h L_\odot \text{ Mpc}^{-3}$  derived by Norberg et al. (2002) using the full 2dFGRS catalogue, with appropriate evolution and  $k$ -corrections applied (up to 17 per cent at the redshifts of the SGP galaxies).

We calculate  $\langle M_{\text{H I}}/L \rangle$  by stacking individual  $M_{\text{H I}}/L$  ‘spectra’. We do so via equations (3) and (4), replacing  $M_{\text{H I}, \nu_{\text{em}, i}}$  with  $M_{\text{H I}, \nu_{\text{em}, i}}/L'_i$ . As discussed in Section 4.2, it is appropriate to restrict the spectral integration range to  $\pm 300 \text{ km s}^{-1}$  from the rest frame since any contribution outside of this is due only to confused sources. We find  $\langle M_{\text{H I}}/L \rangle = 0.43 \pm 0.03 M_\odot/L_\odot$  for the SGP sample, and  $0.72 \pm 0.03 M_\odot/L_\odot$  for the HIPASS sample, where the errors are measured as in Section 3.3.3.

We require the mass-to-light ratio to be weighted by the luminosity density, rather than the luminosity selection function of the input catalogue (hence the subscript  $\rho_L$  in equation 9). We therefore apply a weighting correction to the mean mass-to-light ratio as follows:

$$\left\langle \frac{M_{\text{H I}}}{L'} \right\rangle_{\rho_L} = \left\langle \frac{M_{\text{H I}}}{L'} \right\rangle_s \times \frac{\int N(L) dL}{\int L^\alpha N(L) dL} \times \frac{\int L^\alpha \rho_L(L) dL}{\int \rho_L(L) dL}, \quad (10)$$

where  $\rho_L(L)$  is the luminosity density function and  $N(L)$  is the original luminosity distribution of the input redshift sample. The parameter  $\alpha$  is the power-law dependence of the average H I mass-to-light ratio of galaxies on luminosity in solar units:

$$\frac{M_{\text{H I}}}{L} = \beta L^\alpha. \quad (11)$$

We adopt the  $z = 0$  values  $\alpha = -0.38$  and  $\log \beta = (3.34 - 2\alpha \log h)$  found by Karachentsev et al. (2008) using a subset of HIPASS galaxies with optical counterparts. For the HIPASS sample, the weighting factor applied to the mean mass-to-light ratio is 0.62. For the SGP sample, where galaxies are more luminous and have lower H I mass-to-light ratios, it is 1.35. That is, the mean H I mass-to-light ratio is predicted to be 2.2 times greater for galaxies in the HIPASS sample compared with the SGP sample on the basis of our previous knowledge of the luminosity dependence of  $M_{\text{H I}}/L$ .

We convert  $\rho_{\text{H I}}$  into a fraction of the critical density of the Universe per unit comoving volume,  $\Omega_{\text{H I}}$ , using



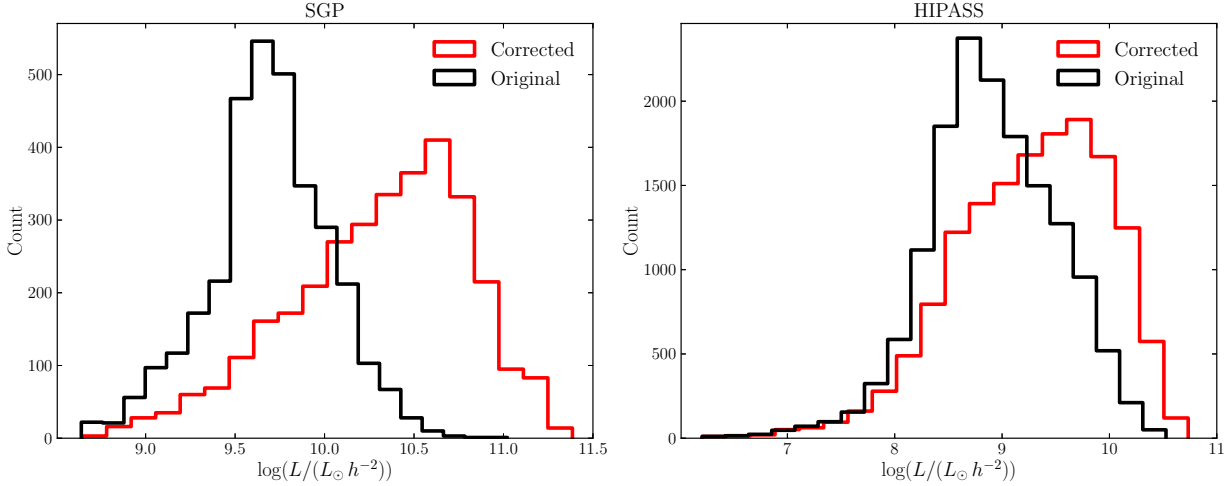


**Figure 7.** The luminosity distribution of all stacked optical sources in the SGP field (left) and HIPASS field (right). The black line represents the original  $b_J$  luminosities of the sample, as defined in the 2dFGRS source catalogue. The red line shows the distribution once luminosities have been adjusted to include a beam-weighted sum of the luminosities of all confused galaxies.

$$\Omega_{\text{H I}} = \frac{8\pi G \rho_{\text{H I}}}{3H_0^2}, \quad (12)$$

where  $G$  is the gravitational constant and  $H_0$  is the Hubble constant. We find  $\Omega_{\text{H I}} = (3.19_{-0.59}^{+0.43}) \times 10^{-4} h^{-1}$  for the  $0.04 < z < 0.13$  SGP data and  $(2.82_{-0.59}^{+0.30}) \times 10^{-4} h^{-1}$  for the  $z < 0.04$  HIPASS data. This implies that there has been no ( $12 \pm 23$  per cent) evolution in the cosmic H I mass density over the past  $1.2 h^{-1}$  Gyr.

The errors in  $\Omega_{\text{H I}}$  are a combination of: (i) the  $\sim 6$  per cent error in  $\langle M_{\text{H I}}/L \rangle$  quoted previously, (ii) a 9 per cent error in  $\rho_L$  and (iii) the 1–11 per cent estimated uncertainty in the confusion correction. The latter was estimated from: (a) variance in  $\langle M_{\text{H I}}/L \rangle$  in different windows from  $\pm 200$  to  $\pm 400 \text{ km s}^{-1}$  over the stacked spectrum and (b) variance in  $\langle M_{\text{H I}}/L \rangle$  calculated using different angular resolutions (and corresponding confusion corrections) in the range 15.5–21.9 arcmin.

Table 2 and Fig. 8 compare the values calculated here to other observational constraints on  $\Omega_{\text{H I}}$  from the literature. Values at look-back times of less than  $4 h^{-1}$  Gyr have been calculated from either direct or stacked 21 cm detections. The Chang et al. (2010) point at  $4.8 h^{-1}$  Gyr was derived using 21 cm intensity mapping. All other points estimate the H I column density of galaxies from the absorption spectra of background QSOs. The evolutionary trends in Fig. 8 are flatter than other examples of this plot in the literature because we have removed the contribution of helium from the values presented in Rao et al. (2006) and Lah et al. (2007) and used the latest DLA measurements of Prochaska & Wolfe (2009) rather than Prochaska et al. (2005).

The  $\Omega_{\text{H I}}$  values we derive here are consistent, within the error margins, with previous estimates over the same redshift range by Zwaan et al. (2005), Martin et al. (2010) and Freudling et al. (2011). It is particularly interesting to note the close agreement between our low-redshift result, derived by stacking HIPASS detections and non-detections, and that of Zwaan et al. (2005), derived from only direct HIPASS detections.

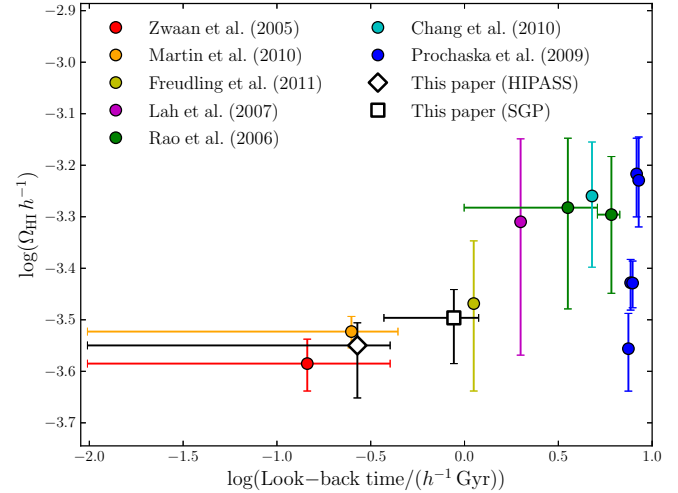


**Figure 8.** Observational constraints on the cosmic H I mass density  $\Omega_{\text{H I}}$  as a function of look-back time. The horizontal error bars indicate the full redshift range over which the measurement applies. The  $\Omega_{\text{H I}}$  estimates using spectral stacking of HIPASS and SGP data are shown as the black diamond and square points, respectively.

It is possible that we have underestimated our uncertainties in the confusion correction. Perhaps, due to evolution, there are more low-mass galaxies in our beam than we have accounted for. Whether or not this is the case will be apparent in future deep studies with radio telescopes with smaller beam sizes. However, it could also be that the other measurements listed have missed galaxies, perhaps because of the difficulty in defining selection functions or extrapolating the H I density function, and are not as accurate as claimed. The use of the stacking method means that the contribution from even low H I mass galaxies is included. Furthermore, as will be apparent in the next section, previous surveys may in fact be completely dominated by cosmic variance.

Source	$\langle z \rangle$	Look-back time ( $h^{-1}$ Gyr)	$\Omega_{\text{HI}} (\times 10^{-4} h^{-1})$
Zwaan et al. (2005)	0.015	0.15	$2.6 \pm 0.3$
<b>This paper (HIPASS)</b>	<b>0.028</b>	<b>0.27</b>	<b><math>2.82^{+0.30}_{-0.59}</math></b>
Martin et al. (2010)	0.026	0.25	$3.0 \pm 0.2$
<b>This paper (SGP)</b>	<b>0.096</b>	<b>0.88</b>	<b><math>3.19^{+0.43}_{-0.59}</math></b>
Freudling et al. (2011)	0.125	1.12	$3.4 \pm 1.1$
Lah et al. (2007) <sup>a</sup>	0.24	1.99	$4.9 \pm 2.2$
Rao et al. (2006) <sup>a,b</sup>	0.505	3.55	$5.2 \pm 1.9$
Chang et al. (2010)	0.80	4.78	$5.5 \pm 1.5$
Rao et al. (2006) <sup>a,b</sup>	1.275	6.07	$5.0 \pm 1.5$
Prochaska & Wolfe (2009) <sup>b</sup>	2.31	7.47	$2.78^{+0.48}_{-0.48}$
Prochaska & Wolfe (2009) <sup>b</sup>	2.57	7.68	$3.73^{+0.41}_{-0.43}$
Prochaska & Wolfe (2009) <sup>b</sup>	2.86	7.87	$3.73^{+0.39}_{-0.39}$
Prochaska & Wolfe (2009) <sup>b</sup>	3.22	8.06	$5.24^{+0.44}_{-0.46}$
Prochaska & Wolfe (2009) <sup>b</sup>	3.70	8.26	$6.07^{+1.05}_{-1.06}$
Prochaska & Wolfe (2009) <sup>b</sup>	4.39	8.48	$5.90^{+1.26}_{-1.11}$

**Table 2.** Observational constraints on  $\Omega_{\text{HI}}$  from the literature. All values have been converted to the same cosmology. The mean redshift and associated look-back time of each sample are quoted. Results presented in this paper are shown in bold. Errors on our values include statistical uncertainty in our stacking analysis, uncertainty in the 2dFGRS luminosity density and systematic errors introduced by correction for confusion. <sup>a</sup> Original values quoted were  $\Omega_{\text{gas}}$  and included a He contribution but have been converted to  $\Omega_{\text{HI}}$  here. (See source for the value of the assumed contribution). <sup>b</sup> Values were calculated using only systems with H I surface densities  $> 2 \times 10^{20} \text{ cm}^{-2}$  (i.e. measures  $\Omega_{\text{HI}}^{\text{DLA}}$ ).

#### 4.4 Cosmic variance

When observations are limited to a finite volume of the Universe, a significant contribution to the error in estimates of cosmological values, such as  $\Omega_{\text{HI}}$ , can come from cosmic variance. That is, variation in galaxy density due to large-scale structure. By employing the stacking technique, we are not restricted to volumes where direct detections are possible. Therefore, the volumes we probe are  $3.7 \times 10^5$  and  $3.4 \times 10^5 h^{-3} \text{ Mpc}^3$  for the SGP and HIPASS samples, respectively. Within the median 2dFGRS redshift range ( $z < 0.11$ ), the SGP volume reduces to  $1.8 \times 10^5 h^{-3} \text{ Mpc}^3$ . These are significantly larger than the sampled volumes of Zwaan et al. (2005) using HICAT ( $8.2 \times 10^4 h^{-3} \text{ Mpc}^3$ , for a median redshift of 0.009), Martin et al. (2010) using the 40 per cent ALFALFA source catalogue ( $1.4 \times 10^5 h^{-3} \text{ Mpc}^3$ , for a median redshift of 0.027) and Freudling et al. (2011) using the AUDS pilot survey ( $7.5 \times 10^2 h^{-3} \text{ Mpc}^3$ ). Furthermore, the luminosity density  $\rho_L$  is calculated by Norberg et al. (2002) from an even higher volume of  $7.3 \times 10^6 h^{-3} \text{ Mpc}^3$ . Therefore, uncertainty in  $\Omega_{\text{HI}}$  due to cosmic variance is dramatically lower in our results than in than any previous sample.

As discussed in Section 3.1, we have chosen a region which is not representative of the average Universe at  $0.04 < z < 0.13$ . Rather, the SGP field contains a small overdensity. The selection of an over-dense region gives a higher volume-integrated H I mass. However, to first order, this should not bias our measurement of the average mass-to-light ratio of galaxies, and therefore the H I mass density we calculate will be a fair estimate of the cosmic value. While the local environment is known to influence the H I properties of galaxies (eg. Haynes et al. 1984), little is known about the relationship between the H I mass-to-light ratio and galaxy density over the very large scales and very low overdensities we probe. For comparison, galaxies in the Virgo Cluster, which has a stellar overdensity two orders of magni-

tude higher than the field (Davies et al. 2012), appear to be four times more H I-deficient compared with background field galaxies (Taylor et al. 2012). Crudely assuming that the interaction rate between galaxies (as for gaseous particles) is proportional to the product of density and velocity dispersion, an overdensity of 30 per cent will only lead to an H I deficiency of 1 per cent or so.

#### 4.5 Binning

We now investigate H I trends with redshift, luminosity and colour. We split the parent sample into bins containing roughly equal source counts. We then stack the mass spectra of all sources within each subsample. By splitting the SGP parent sample into three bins and the HIPASS sample into eight bins, we can still achieve a statistically significant detection in each. Tables 3 and 4 show the properties of each SGP and HIPASS subsample, respectively. The variation of the average H I mass and mass-to-light ratio in each bin is plotted in Fig. 9.

To minimize confusion in our results, we have restricted the measurement of both  $\langle M_{\text{HI}} \rangle$  and  $\langle M_{\text{HI}}/L \rangle$  to the  $\pm 300 \text{ km s}^{-1}$  spectral range, as in Section 4.3. We have adjusted the luminosities to account for confusion (via equation 8) before binning. We have also used these corrected luminosities ( $L'$ ) to determine the mass-to-light ratios. Note, however, that it is not appropriate to apply the  $M_{\text{HI}}/L$  weighting (equation 10) to this binning analysis.

The average H I mass-to-light ratios we measure are consistent with the results of Doyle et al. (2005) who study HIPASS galaxies with optical counterparts identified in the 6dF Galaxy Survey. They find that the  $b_J$ -band mass-to-light ratios of these galaxies are predominantly less than  $5 M_{\odot}/L_{\odot}$ . For comparison, the highest mass-to-light ratio we measure is  $2.0 \pm 0.2 M_{\odot}/L_{\odot}$  and is associated with the lowest HIPASS luminosity bin.

We find that the H I mass increases and the mass-to-

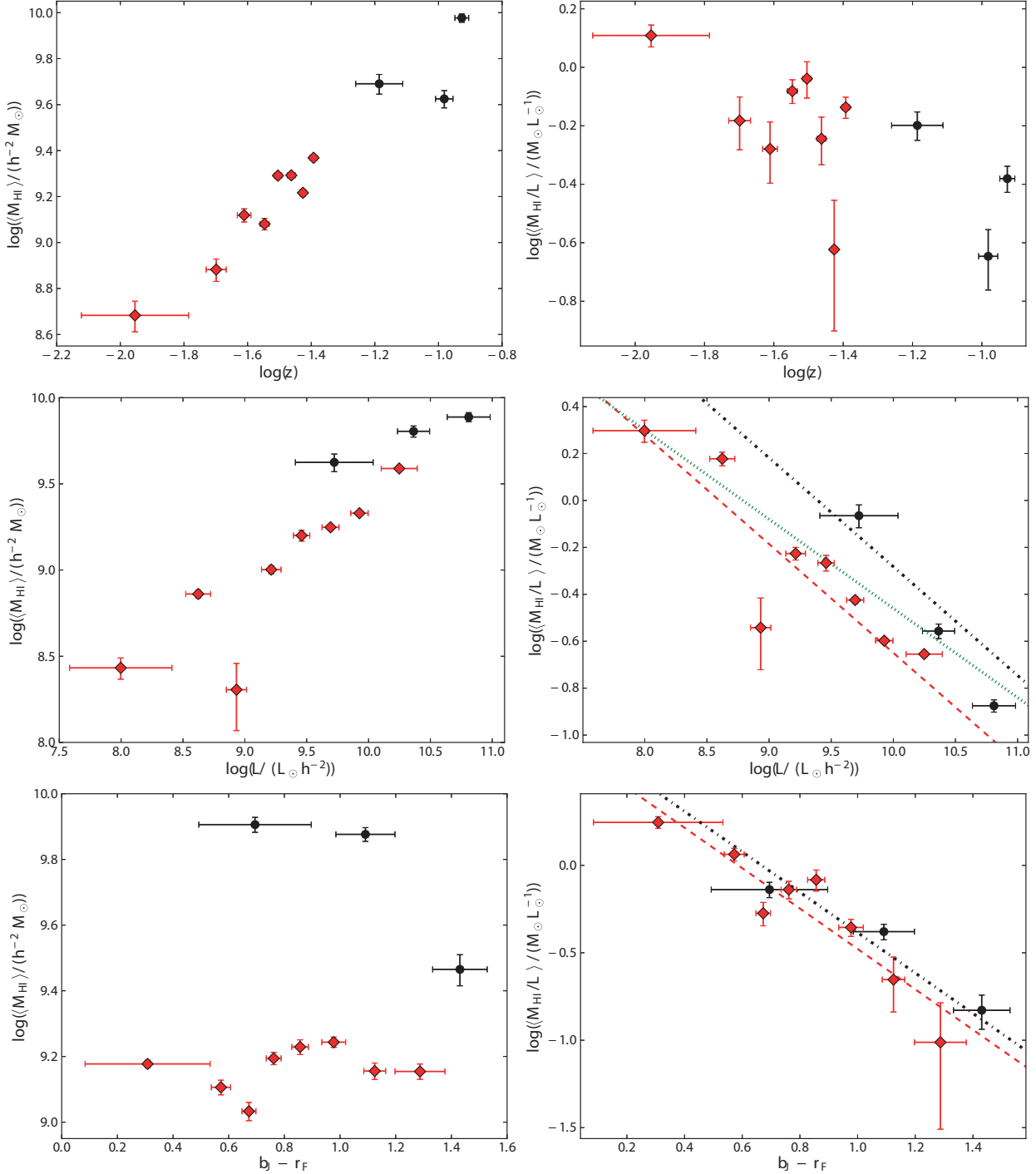


**Figure 9.** The average H I masses (left) and average mass-to-light ratios (right) derived by co-adding all spectra in bins of (from top to bottom) redshift,  $b_J$  luminosity and  $(b_J - r_F)$  colour. The values are plotted at the mean value of the binned parameter in each subsample. The error bars represent the  $1\sigma$  spread within the bin. Values derived from SGP data are shown as black points, while the HIPASS values are shown as red diamonds. The red dashed lines in the two lower-right panels show the least-squares fit to the HIPASS points. The black dot-dashed lines show the fit to the SGP points, assuming the same gradient as the HIPASS fit. The green dotted line shows the relationship between  $M_{\text{HI}}/L$  and luminosity as estimated by Karachentsev et al. (2008).

light ratio decreases with  $b_J$  luminosity in both the HIPASS and SGP samples. The former reflects the fact that more luminous galaxies are often larger in size and therefore contain greater total H I masses (eg. Toribio et al. 2011). The fact that lower optical luminosity galaxies have higher mass-

to-light ratios has been well established through direct H I observations (eg. Warren et al. 2006) and we have verified here that such trends can be reproduced with a stacking analysis.

We have performed a least-squares linear fit to the

Property	Bin range	Mean	rms	$N$	Integrated S/N	Peak S/N	$\langle M_{\text{H I}} \rangle (\times 10^9 h^{-2})$	$\langle M_{\text{H I}}/L' \rangle$
$z$	0.0406 – 0.0863	0.0651	0.0111	1082	10.2	4.8	$4.90 \pm 0.48$	$0.63 \pm 0.07$
	0.0863 – 0.1116	0.1043	0.0066	1099	11.6	4.8	$4.21 \pm 0.36$	$0.22 \pm 0.05$
	0.1116 – 0.1318	0.1184	0.0059	1096	23.5	9.0	$9.48 \pm 0.40$	$0.42 \pm 0.04$
$\log(L'/(L_{\odot} h^{-2}))$	8.645 – 10.122	9.723	0.314	1082	8.5	5.5	$4.22 \pm 0.50$	$0.86 \pm 0.10$
	10.122 – 10.576	10.364	0.129	1081	13.5	7.1	$6.38 \pm 0.47$	$0.28 \pm 0.02$
	10.576 – 11.385	10.810	0.174	1114	16.7	6.4	$7.72 \pm 0.46$	$0.13 \pm 0.01$
$(b_J - r_F)$	-1.699 – 0.918	0.695	0.2019	1083	19.0	10.6	$8.05 \pm 0.42$	$0.73 \pm 0.07$
	0.918 – 1.271	1.091	0.1061	1081	20.7	7.6	$7.52 \pm 0.36$	$0.42 \pm 0.04$
	1.271 – 2.089	1.431	0.0980	1113	9.2	3.0	$2.92 \pm 0.32$	$0.15 \pm 0.03$

**Table 3.** Binned parameters for the SGP data. Columns (from left to right) are: the binned property, bin range, mean and rms within the bin range, number of sources, integrated and peak signal-to-noise ratio of the stacked mass spectrum, average mass (units  $M_{\odot}$ ) and average mass-to-light ratio (units  $M_{\odot}/L_{\odot}$ ) calculated from the stacked spectrum.

Property	Bin range	Mean	rms	$N$	Integrated S/N	Peak S/N	$\langle M_{\text{H I}} \rangle (\times 10^9 h^{-2})$	$\langle M_{\text{H I}}/L' \rangle$
$z$	0.0026 – 0.0171	0.0111	0.0043	1814	6.6	4.0	$0.48 \pm 0.07$	$1.28 \pm 0.11$
	0.0171 – 0.0224	0.0200	0.0014	1981	9.0	6.4	$0.77 \pm 0.09$	$0.66 \pm 0.13$
	0.0224 – 0.0265	0.0245	0.0012	1814	15.1	12.2	$1.32 \pm 0.09$	$0.53 \pm 0.12$
	0.0265 – 0.0298	0.0284	0.0009	1964	17.3	9.8	$1.12 \pm 0.07$	$0.83 \pm 0.08$
	0.0298 – 0.0327	0.0313	0.0008	1799	33.7	13.8	$1.96 \pm 0.06$	$0.94 \pm 0.13$
	0.0327 – 0.0361	0.0345	0.0010	1986	36.7	15.2	$1.97 \pm 0.05$	$0.57 \pm 0.11$
	0.0361 – 0.0388	0.0374	0.0008	1798	28.0	11.1	$1.65 \pm 0.06$	$0.24 \pm 0.11$
	0.0388 – 0.0423	0.0405	0.0010	1937	70.2	17.4	$2.35 \pm 0.03$	$0.73 \pm 0.06$
$\log(L'/(L_{\odot} h^{-2}))$	6.206 – 8.426	7.997	0.413	1812	7.1	7.3	$0.30 \pm 0.04$	$1.98 \pm 0.201$
	8.426 – 8.787	8.623	0.101	1963	19.8	6.8	$0.73 \pm 0.04$	$1.51 \pm 0.10$
	8.787 – 9.073	8.932	0.082	1810	2.4	5.4	$0.20 \pm 0.09$	$0.29 \pm 0.10$
	9.073 – 9.345	9.214	0.079	1962	18.3	11.0	$1.01 \pm 0.06$	$0.59 \pm 0.04$
	9.345 – 9.574	9.459	0.066	1811	13.8	12.3	$1.59 \pm 0.12$	$0.54 \pm 0.04$
	9.574 – 9.809	9.683	0.069	1962	26.3	12.1	$1.77 \pm 0.07$	$0.37 \pm 0.01$
	9.809 – 10.050	9.927	0.070	1811	34.1	14.8	$2.13 \pm 0.06$	$0.25 \pm 0.01$
	10.050 – 10.734	10.248	0.146	1962	39.1	19.2	$3.88 \pm 0.10$	$0.22 \pm 0.01$
$(b_J - r_F)$	-0.994 – 0.504	0.309	0.224	1814	37.7	13.5	$1.51 \pm 0.04$	$1.76 \pm 0.13$
	0.504 – 0.629	0.572	0.035	1965	19.5	13.4	$1.28 \pm 0.07$	$1.16 \pm 0.10$
	0.629 – 0.716	0.673	0.025	1816	15.7	12.9	$1.08 \pm 0.07$	$0.53 \pm 0.08$
	0.716 – 0.807	0.762	0.027	1956	23.1	13.0	$1.57 \pm 0.07$	$0.73 \pm 0.08$
	0.807 – 0.908	0.856	0.030	1814	19.4	12.4	$1.70 \pm 0.09$	$0.83 \pm 0.11$
	0.908 – 1.056	0.977	0.043	1955	27.8	12.8	$1.76 \pm 0.06$	$0.44 \pm 0.05$
	1.056 – 1.190	1.125	0.039	1817	17.3	9.6	$1.44 \pm 0.08$	$0.22 \pm 0.08$
	1.190 – 1.958	1.287	0.090	1956	18.6	9.8	$1.43 \pm 0.08$	$0.10 \pm 0.07$

**Table 4.** Binned parameters for the HIPASS data. Columns are as defined in Table 3.

HIPASS data, as shown in Fig. 9. Fitting to the SGP data is less robust, owing to the small number of bins. However, we perform the linear fit assuming the same gradient as the HIPASS fit. The dotted line in Fig. 9 shows the close match of the mass-to-light versus luminosity derived by Karachentsev et al. (2008), compared with our results (see also Table 5). This verifies our adjustment for the luminosity dependence of the mass-to-light ratio. The only SGP point to substantially deviate is the lowest luminosity bin, which is the main reason for the slightly increased value of  $\Omega_{\text{H I}}$  in Table 2.

Similar H I trends are seen with redshift. This does not reveal any real evolution, but arises because we do not have a volume-limited sample and are therefore preferentially detecting the higher mass and luminosity galaxies at higher

redshifts. It is precisely this bias that we are attempting to correct via equation (10) in our above calculation of the H I mass density.

We use the SuperCOSMOS  $b_J$  and  $r_F$  magnitudes, as defined in the 2dFGRS catalogue, to examine trends with colour. For the SGP population, which contains high-mass galaxies in each colour bin, a higher total H I mass is seen for bluer sources. The HIPASS sample contains a range of masses at all colours, and it is therefore unfair to directly compare the H I masses in each bin. The large vertical offset between the two samples can again be explained by the preferential inclusion of higher mass sources in the SGP sample due to the magnitude limits of the optical catalogue.

Taking the ratio with the optical luminosity removes the galaxy size dependence, revealing a clear relationship

$x$	HIPASS		SGP	(Karachentsev et al. 2008)	
	$a$	$b$	$b$	$a$	$b$
$\log(L'/(L_{\odot} h^{-2}))$	-0.46	4.00	4.35	-0.38	3.34
$(b_J - r_F)$	-1.15	0.68	0.77	-	-

**Table 5.** Parameters for the lines in Fig. 9 showing the derived relationships between H I mass-to-light ratio and luminosity and colour:  $\log(\langle M_{\text{H I}}/L' \rangle) = ax + b$ . The fit to the SGP points has been derived using the HIPASS gradient; hence, only the offset is quoted.

between the H I mass-to-light ratio and colour. We see that bluer sources have higher mass-to-light ratios. Again, we perform a linear fit to the HIPASS data, and apply this gradient to the SGP fit. Both data sets are remarkably consistent and reflect similar trends found between colour and gas fraction in previous studies using both direct H I detections (eg. Spitzak & Schneider 1998) and 21 cm stacking experiments (Fabello et al. 2011a). This supports the notion that galaxies with larger gas supplies are generally associated with increased star formation.

Much of the colour dependence reflects the colour-magnitude relation and is therefore corrected for in our calculation of  $\Omega_{\text{H I}}$ , which incorporates a luminosity correction to  $M_{\text{H I}}/L$ . However, it is possible that there remain residual differences between galaxies in the SGP and HIPASS samples. For example, Li et al. (2012) examined the residual dependence of H I-to-stellar mass ratio on a number of parameters, and found that a simultaneous dependence on stellar mass and colour (as well surface brightness and colour gradient) best explains the properties of luminous SDSS galaxies. However, after application of the luminosity correlation in Table 5, we find no residual dependence of  $M_{\text{H I}}/L$  on colour to an accuracy of 10 per cent over the mean colour difference between SGP and HIPASS galaxies.

## 5 CONCLUSIONS

We have presented an H I spectral stacking analysis of galaxies identified in the 2dFGRS. We have shown that H I stacking can be used to efficiently and accurately probe the statistical properties of high-redshift field galaxies.

Our sample consists of 15,093 galaxies at  $0.0025 < z < 0.0423$  and 3,277 galaxies at  $0.0405 < z < 0.1319$ . 21 cm data for the low-redshift sample were provided by HIPASS. For the high-redshift sample, new 21 cm observations of a 42 deg<sup>2</sup> field near the SGP were conducted with the Parkes radio telescope. Many of the low-redshift optical galaxies are found to have strong H I signatures, consistent with the HICAT. Only one galaxy is detected above the  $5\sigma$  limit in the SGP sample.

We have co-added the H I spectra of all galaxies in our sample, after aligning each at the rest frame. We thus report a strong  $31\sigma$  average detection of the HIPASS galaxies and a  $12\sigma$  detection for the SGP galaxies. The sensitivity level we achieve for our stacked spectra is equivalent to observing a single object for  $\sim 37$  d. Therefore, we have shown that spectral stacking is an effective method of making statistical detections of large numbers of individually undetected galaxies at high redshift with reasonable integration times.

The rms noise in the stacked signal displays Gaussian behaviour, decreasing with the square root of the number of

co-added spectra. We find no apparent intrinsic limitation in the depth to which we can continue stacking experiments with the Parkes telescope. This bodes well for future stacking experiments with deep, large-scale H I surveys on the next generation of radio telescopes such as the Australian SKA Pathfinder, MeerKAT, APERTIF and ultimately the SKA.

We measure an average H I mass of  $\langle M_{\text{H I}} \rangle = (1.48 \pm 0.03) \times 10^9 h^{-2} M_{\odot}$  from the HIPASS stacked spectrum and  $\langle M_{\text{H I}} \rangle = (6.93 \pm 0.17) \times 10^9 h^{-2} M_{\odot}$  from the SGP stacked spectrum. However, we find that these averages, particularly that of the SGP sample, are over estimated due to source confusion. High-resolution follow-up observations to combat this issue are underway with the Australia Telescope Compact Array and will be presented in a future paper.

For now, we employ the Tully-Fisher relation to estimate source line widths and thus to predict the extent of confusion in our data. We then adjust the optical luminosities to include a beam-weighted sum of all confused galaxies. Finding the average mass-to-light ratio and accounting for sample bias, we derive the cosmic H I mass density ( $\Omega_{\text{H I}}$ ). We find  $\Omega_{\text{H I}} = (2.82^{+0.30}_{-0.59}) \times 10^{-4} h^{-1}$  at  $0 < z < 0.04$  and  $(3.19^{+0.43}_{-0.59}) \times 10^{-4} h^{-1}$  at  $0.04 < z < 0.13$ , i.e. we find no ( $12 \pm 23$  per cent) evolution over the past  $\sim 1 h^{-1}$  Gyr. Within the error margins, these values agree with previous  $\Omega_{\text{H I}}$  estimates made via direct detections in the HIPASS, ALFALFA and AUDES surveys. We argue that our results are far more robust to cosmic variance.

Finally, we employ the stacking technique to investigate the variation of H I properties with redshift, luminosity and colour. Trends seen with redshift are obscured by selection effects. We find that lower luminosity galaxies have lower total H I masses but higher mass-to-light ratios. We also see a decrease in the mass-to-light ratio from blue to red galaxies. These results agree with direct observations.

## ACKNOWLEDGEMENTS

We are grateful to staff at the Parkes radio telescope for technical support, particularly Ettore Carretti and Stacy Mader. Thanks to Morag Scrimgeour and Chris Harris for observing assistance. The Parkes radio telescope is part of the Australia Telescope National Facility which is funded by the Commonwealth of Australia for operation as a National Facility managed by CSIRO. We acknowledge the efforts of the 2dFGRS and HIPASS collaborations. JD wishes to thank the International Centre for Radio Astronomy Research for funding support, Laura Hoppmann and Stefan Westerlund for coding assistance and Tobias Westmeier, Aaron Robotham, Chris Power, Martin Zwaan, Marc Verheijen and Jason Prochaska for useful discussions. Parts of this

research were conducted by the Australian Research Council Centre of Excellence for All-sky Astrophysics (CAAS-TRO), through project number CE110001020. We acknowledge the use of the TOPCAT software in our data analysis (<http://www.starlink.ac.uk/topcat/>).

## References

- Barnes D. G. et al., 2001, *Monthly Notices of the Royal Astronomical Society*, 322, 486
- Catinella B., Haynes M. P., Giovanelli R., Gardner J. P., Connolly A. J., 2008, *The Astrophysical Journal Letters*, 685, L13
- Cen R., Ostriker J. P., Prochaska J. X., Wolfe A. M., 2003, *The Astrophysical Journal*, 598, 741
- Chang T.-C., Pen U.-L., Bandura K., Peterson J. B., 2010, *Nature*, 466, 463
- Chengalur J. N., Braun R., Wieringa M., 2001, *Astronomy and Astrophysics*, 372, 768
- Colless M. et al., 2001, *Monthly Notices of the Royal Astronomical Society*, 328, 1039
- Condon J. J., Cotton W. D., Greisen E. W., Yin Q. F., Perley R. A., Taylor G. B., Broderick J. J., 1998, *The Astronomical Journal*, 115, 1693
- Davies J. I. et al., 2012, *Monthly Notices of the Royal Astronomical Society*, 419, 3505
- Doyle M. T. et al., 2005, *Monthly Notices of the Royal Astronomical Society*, 361, 34
- Eke V. R. et al., 2004, *Monthly Notices of the Royal Astronomical Society*, 348, 866
- Fabello S., Catinella B., Giovanelli R., Kauffmann G., Haynes M. P., Heckman T. M., Schiminovich D., 2011a, *Monthly Notices of the Royal Astronomical Society*, 411, 993
- Fabello S., Kauffmann G., Catinella B., Giovanelli R., Haynes M. P., Heckman T. M., Schiminovich D., 2011b, *Monthly Notices of the Royal Astronomical Society*, 416, 1739
- Fall S. M., Pei Y. C., 1993, *The Astrophysical Journal*, 402, 479
- Freudling W. et al., 2011, *The Astrophysical Journal*, 727, 40
- Giovanelli R. et al., 2005, *The Astronomical Journal*, 130, 2598
- Haynes M. P., Giovanelli R., Chincarini G. L., 1984, *Annual Review of Astronomy and Astrophysics*, 22, 445
- Hopkins A. M., Beacom J. F., 2006, *The Astrophysical Journal*, 651, 142
- Karachentsev I. D., Makarov D. I., Karachentseva V. E., Melnik O. V., 2008, *Astronomy Letters*, 34, 832
- Kereš D., Katz N., Weinberg D. H., Davé R., 2005, *Monthly Notices of the Royal Astronomical Society*, 363, 2
- Lagos C. D. P., Baugh C. M., Lacey C. G., Benson A. J., Kim H.-S., Power C., 2011, *Monthly Notices of the Royal Astronomical Society*, 418, 1649
- Lah P. et al., 2007, *Monthly Notices of the Royal Astronomical Society*, 376, 1357
- Lah P. et al., 2009, *Monthly Notices of the Royal Astronomical Society*, 399, 1447
- Li C., Kauffmann G., Fu J., Wang J., Catinella B., Fabello S., Schiminovich D., Zhang W., 2012, *Monthly Notices of the Royal Astronomical Society*, 424, 1471
- Madau P., Ferguson H. C., Dickinson M. E., Giavalisco M., Steidel C. C., Fruchter A., 1996, *Monthly Notices of the Royal Astronomical Society*, 283, 1388
- Martin A. M., Papastergis E., Giovanelli R., Haynes M. P., Springob C. M., Stierwalt S., 2010, *The Astrophysical Journal*, 723, 1359
- Masui K. W. et al., 2013, *The Astrophysical Journal Letters*, 763, L20
- Meyer M. J., Zwaan M. A., Webster R. L., Schneider S., Staveley-Smith L., 2008, *Monthly Notices of the Royal Astronomical Society*, 391, 1712
- Meyer M. J. et al., 2004, *Monthly Notices of the Royal Astronomical Society*, 350, 1195
- Nagamine K., Cen R., Hernquist L., Ostriker J. P., Springel V., 2005, *The Astrophysical Journal*, 618, 23
- Norberg P. et al., 2002, *Monthly Notices of the Royal Astronomical Society*, 336, 907
- Obreschkow D., Ma X., Meyer M., Power C., Zwaan M., Staveley-Smith L., Drinkwater M. J., 2013, *The Astrophysical Journal*, 766, 137
- Pen U.-L., Staveley-Smith L., Peterson J. B., Chang T.-C., 2009, *Monthly Notices of the Royal Astronomical Society*, 394, L6
- Power C., Baugh C. M., Lacey C. G., 2010, *Monthly Notices of the Royal Astronomical Society*, 406, 43
- Prochaska J. X., Herbert-Fort S., Wolfe A. M., 2005, *The Astrophysical Journal*, 635, 123
- Prochaska J. X., Wolfe A. M., 2009, *The Astrophysical Journal*, 696, 1543
- Rao S. M., Turnshek D. A., Nestor D. B., 2006, *The Astrophysical Journal*, 636, 610
- Somerville R. S., Primack J. R., Faber S. M., 2001, *Monthly Notices of the Royal Astronomical Society*, 320, 504
- Spitzak J. G., Schneider S. E., 1998, *The Astrophysical Journal Supplement Series*, 119, 159
- Staveley-Smith L. et al., 1996, *Publications of the Astronomical Society of Australia*, 13, 243
- Taylor R., Davies J. I., Auld R., Minchin R. F., 2012, *Monthly Notices of the Royal Astronomical Society*, 423, 787
- Toribio M. C., Solanes J. M., Giovanelli R., Haynes M. P., Martin A. M., 2011, *The Astrophysical Journal*, 732, 93
- Verheijen M., van Gorkom J. H., Szomoru A., Dwarakanath K. S., Poggianti B. M., Schiminovich D., 2007, *The Astrophysical Journal Letters*, 668, L9
- Warren B. E., Jerjen H., Koribalski B. S., 2006, *The Astronomical Journal*, 131, 2056
- Wong O. I. et al., 2006, *Monthly Notices of the Royal Astronomical Society*, 371, 1855
- Zwaan M. A., 2000, PhD thesis, PhD Thesis, Groningen: Rijksuniversiteit, 2000 152 p. Proefschrift, Rijksuniversiteit Groningen, 2000
- Zwaan M. A., Meyer M. J., Staveley-Smith L., Webster R. L., 2005, *Monthly Notices of the Royal Astronomical Society*, 359, L30
- Zwaan M. A., van Dokkum P. G., Verheijen M. A. W., 2001, *Science*, 293, 1800